Data-Driven Modeling and Design of Multi-variable Dynamic Sliding Mode Control for the Underground Coal Gasification Project Thar

Article *in* IEEE Transactions on Control Systems Technology · January 2021

DOI: 10.1109/TCST.2021.3057633

CITATIONS
6

READS
115

5 authors, including:

Syed Bilal Javed
National Engineering & Scientific Commission, Islamabad, Pakistan
11 PUBLICATIONS **47** CITATIONS
SEE PROFILE

Ali Arshad
COMSATS University Islamabad
39 PUBLICATIONS **364** CITATIONS
SEE PROFILE

Raza Samar
Capital University of Science & Technology
71 PUBLICATIONS **1,419** CITATIONS
SEE PROFILE

Aamer Iqbal Bhatti
University of Engineering & Technology Lahore
245 PUBLICATIONS **2,091** CITATIONS
SEE PROFILE

Data-Driven Modeling and Design of Multi-variable Dynamic Sliding Mode Control for the Underground Coal Gasification Project Thar

Syed B. Javed[1], Vadim I. Utkin[2], *Fellow, IEEE*, Ali A. Uppal[3], *Member, IEEE*, Raza Samar[4], *Member, IEEE*, Aamer I. Bhatti[5], *Senior Member, IEEE*

***Abstract*—The energy output per unit time is an important performance metric to determine the potential of an underground coal gasification (UCG) site for electricity production. The energy output per unit time is a function of heating value and flow rate of syngas, and therefore, it is essential to devise a multi-variable closed-loop system to enhance the efficiency of the UCG process. In this work, a model-based, multi-variable dynamic sliding mode control (DSMC) has been designed for the cavity simulation model (CAVSIM), parametrized with the operating parameters and coal properties of the underground coal gasification project Thar (UPT) field. The model-based control of CAVSIM is not possible due to its complex and multidimensional dynamics, thus a simple linear multi-variable model is identified by employing a subspace (N4SID) system identification technique. The regular form of the linear model is formulated to design the model-based dynamic sliding mode control (DSMC). Moreover, the stability of zero dynamics is shown on the approximate model of CAVSIM. Consequently, the designed controller is implemented on CAVSIM, and simulation results are compared with conventional SMC. It has been observed that both the controllers have achieved the tracking objectives in the presence of input disturbance and modeling uncertainties. However, DSMC utilizes lesser control energy to achieve the desired objectives. Furthermore, the continuous control inputs in DSMC significantly reduce chattering.**

***Index Terms*—Data-driven modeling, dynamic sliding mode control, zero dynamics, energy conversion system and underground coal gasification.**

I. Introduction

The International Energy Agency reported that global demand for electricity would rise by 2.1 percent per annum by 2040, resulting in an increase in the electricity demand by approximately 64% [1]. Currently, the share of coal in electricity generation is the highest (38%) amongst all the fuel sources, and it will remain the largest contributor by the year 2040 [1]. The combustion of coal has detrimental impact on the environment, and it is a major cause in global warming. However, various clean coal technologies with integrated gasification combined cycle (IGCC) and/or carbon capture and storage (CCS) system are employed to address the environmental concerns [2]–[5]. Underground coal gasification (UCG) is a clean coal technology, and have several advantages over the surface gasification, such as elimination of coal mining and ash handling, resulting in an increase in the worker's safety and health, low water consumption, reduction in greenhouse gas emission, noise and dust pollution. While UCG is the only option for the low rank and deeply located coal reserves, which are economically infeasible to mine [6], [7].

The planning commission of Pakistan has initiated UCG Project Thar (UPT) in Block V of Thar coal fields located in Sindh [7], [8]. The geological and hydrological conditions in Thar and coal bed properties are best suited to employ UCG technique. The primary objective of this project is to develop a UCG based power plant, which will help to meet the energy demand of the country [7], [9]. In industrial applications like IGCC, energy output per unit time is an important parameter to determine the performance of a UCG field [10]. As the process occurs insitu, it is difficult to develop a monitoring system for the real time data acquisition of geological and hydrological parameters, and the installation of such a monitoring system in itself is a challenging task. Like other UCG fields, UPT has real time monitoring system to measure the composition, temperature, flow rate and pressure of inlet and outlet gases. The only tunning knobs to increase the energy output per unit time are the composition and flow rate of inlet gas.

A. Related work

The development of a closed-loop system for the UCG field is an emerging area of research. For any UCG site, the development of a control system is a formidable task due to numerous challenges, like lack of instrumentation, installation of sensors at different locations, underground disturbances, process nonlinearities, limited tuning knobs and lack of direct control over the process parameters. In the literature, model-free and model-based techniques are used to develop a UCG control system. In [11]–[13], conventional PID controllers have been designed for the UCG process to control the temperature, concentrations and heating value of syngas. An optimal control design to maximize the concentration of CO is also proposed for the similar UCG system [14]. In [15], authors have designed a multi-variable adaptive model predictive

S. B. Javed[1] and A. A. Uppal[3] are with the Department of Electrical and Computer Engineering, COMSATS University Islamabad, Islamabad 44000, Pakistan. S. B. Javed is also a PhD scholar at Capital University of Science and Technology, Islamabad Expressway, Kahuta Road, Zone-V, Islamabad, Pakistan. e-mail: syedbilal@comsats.edu.pk; ali_arshad@comsats.edu.pk

V. I. Utkin[2] is with the Electrical and Computer Engineering Department, The Ohio State University, Columbus, OH 43210 USA (e-mail: utkin.2@osu.edu).

R. Samar[4] and A. I. Bhatti[5] are with the Electrical Engineering Department, Capital University of Science and Technology, Islamabad Expressway, Kahuta Road, Zone-V, Islamabad, Pakistan (e-mail: raza.samar@cust.edu.pk; aib@cust.edu.pk).

control for the laboratory scale UCG setup. The models for the syngas heating value and underground temperature have been developed by using experimental data. The proposed multi-variable control design is not applicable at the field scale UCG, as the real time monitoring of underground temperature is not possible at the UCG site. The laboratory-scale experiments are not sufficient to reflect the actual UCG field [16]. In [11]–[15], all the control designs have been proposed for a laboratory-scale UCG setup, which can not be employed on the actual UCG field.

In the literature, the model-based control technique has been employed for the field scale UCG setup in order to control the heating value of syngas, [9], [17]–[21]. In [9], authors have used an ordinary differential equations (ODEs) to formulate the UCG model. The proposed model is employed to design a sliding mode control by using an equivalent control method. The model has been formulated with an unrealistic assumption that all the states are measurable. The desired heating value of syngas has been achieved by varying the flow rate of inlet gas. In [17], [18], Uppal et al. have used the same model to propose integral sliding mode and dynamic integral sliding mode controllers to maintain the desired trajectory of the heating value. Moreover, a gain-scheduled modified Utkin observer has been designed for the estimation of states, and the robustness of proposed techniques have been shown against an input disturbance, parametric uncertainties and measurement noise.

In [19], partial differential equations (PDEs) are used to develop a control oriented UCG model. The composition and heating value of product gas are determined as a function of various operating parameters and coal bed properties. Moreover, three stoichiometric coefficients of coal pyrolysis reaction have been optimized by using a constrained nonlinear optimization technique. In [20], [21], authors have designed super twisting and conventional sliding mode controllers to maintain desired heating value of the syngas. The model of [19] is used to design both the controllers. In [22], authors have proposed a linear model to design the robust multi-objective H_2/H_∞ control design in order to achieve the desired level of syngas heating value.

B. Gap analysis

In the literature, heating value of syngas is considered only as a key indicator to determine the performance of a UCG field. Thus, authors have considered a single control objective, in which the heating value of syngas is maintained at the desired level by varying the flow rate of inlet gas. While the authors have ignored the flow rate of syngas, which has also significant role to determine the potential of a UCG site to produce electricity. Moreover, most of the control designs depend on nonlinear process models, resulting in a highly complex control system which requires large computational resources and cost. Hence, it is essential to design a multi-variable, model-based control system for the UPT field.

The UPT field lacks the monitoring system to measure the hydrological and geological parameters, such as water influx rate, cavity evolution and its interaction with overburden. In our previous work [8], a 3D axisymmetric cavity simulation model (CAVSIM), developed by Lawrence Livermore National Laboratory (LLNL) USA [23], has been parametrized and validated with the UPT field data. CAVSIM and 1D packed bed model [19] results are compared with the UPT field data for the heating value and composition of syngas, and it has been shown that the CAVSIM results are more accurate than 1D packed bed model.

CAVSIM is more accurate and has already been applied to many UCG fields, but it is highly complex resource recovery model [16].

C. Major contributions

As described earlier, CAVSIM is as an essential simulation tool for UPT field, and it is used for the prediction of important process parameters which are not measurable at the site. However, the complexity of CAVSIM is a major challenge in the designing of model-based multi-variable control system for UPT field. Thus, a simple control-oriented, multi-variable linear model has been identified by using a system identification technique. CAVSIM has been used as a benchmark for generating the input-output data. The linear state-space model has been identified by using subspace (N4SID) method in system identification toolbox of MATLAB. The inlet gas flow rate and steam to oxygen ratio $(H_2O(g)/O_2(g))$ are two inputs of the identified model. While the composition and heating value of syngas are considered as two outputs. Then a linear model is employed to design a multi-variable dynamic sliding mode control (DSMC) in order to attain the desired levels of the outputs. Prior to the implementation of designed controller on the actual model, it is essential to prove that the zero dynamics of the CAVSIM is bounded. As the dynamics of CAVSIM is very complex, and it is not possible to analytically prove the stability of the 3D PDEs. Therefore, a simple 1D packed bed model of the UPT field [19], which preserves the fundamental dynamics of CAVSIM [8], is used to prove the boundedness of the multi-variable UCG process. In this work, the model of [19] is slightly modified to represent the MIMO UCG process model. Finally, the simulation results of DSMC are compared with the conventional SMC, given in [24].

The rest of the article is organized in the following manner. Problem statement is described in Section II, followed by a system identification technique to formulate a linear model in Section III. The control design and approximate model of CAVSIM are described in Section IV and Section V, respectively. The implementation of designed DSMC on CAVSIM is explained in SectionVI. In Section VII, simulation results are discussed, and finally the paper is concluded in Section VIII.

II. Problem Statement

To design a model-based multi-variable DSMC for the UPT field in order to maintain the desired levels of the heating value and flow rate of syngas by manipulating the concentration of injected steam and inlet gas flow rate. The only tuning knobs to attain the desired levels of the outputs are the composition and flow rate of inlet gas, which have been used as control inputs. Moreover, the designed control law must be capable

to cater the effect of external disturbance, and the modeling errors caused by the linearization.

III. Identification of Linear Model

In this work, the actual model is highly complex and the design of model-based multi-variable control is a formidable task. Thus, a system identification technique is employed to formulate a control oriented model for the UPT field. The process of building a model comprises of three main steps; acquiring of experimental data, model estimation and validation with independent data [25]. The data acquired for system identification has paramount significance, and it must reflect the fundamental dynamics of the process. Hence, a careful design of identification experiment is essential, which include the selection of sampling time and an input signal with suitable spectrum. Moreover, it is often necessary to perform a pre-process in order to remove trends, offsets and outliers from the acquired data. After acquiring the data, the most challenging task in model estimation is the selection of an appropriate model structure, which includes the selection of variables, model type and order of model. Finally, the model is validated with another data and residual analysis is also performed to finalize the model [25].

The input-output data acquisition from an industrial process is the foremost challenge in an identification process due to the experimental and economical constraints associated with the conduction of field trials [25]–[27]. UCG is a slow process, as it has a low consumption rate of coal and char. Moreover, the cavity growth and chemical reaction rates are low. The cavity growth rate of various UCG fields are reported in [28], and it is observed that the cavity growth rate is in a range of 0.35m/day to 1.2m/day. However, these rates are the functions of operating conditions and coal bed properties of the UCG site. The coal consumption rate for the UPT field is 0.1-0.2 m/hr [7]. As the UCG process has slow dynamics and the process variables like inlet gas flow rate, pressure and steam to oxygen ratio $H_2O(g)/O_2(g)$ have to be maintained within the safe operating range. Thus, it is not possible to perform identification experiments at the UPT field. For that purpose, CAVSIM simulator is used which has already been validated with the field data of UPT in our previous work [8].

A. Preliminary identification experiments

Prior to design an identification experiment, the information about operating range and nonlinear plant parameters such as delays, time constants, static gains and bandwidth is gathered by performing preliminary step and staircase experiments in both directions [25], [29], [30]. The selection of operating point has a key role in the identification process, and it is determined by performing series of staircase experiments as shown in Fig. 1. The selection of operating point outside the linear range of the process may cause large modeling errors, resulting in a poor estimation of the model [30]. The input and output ranges for the linear region are indicated in Fig. 1, and are given in (1).

$$\begin{aligned} 0.33 \leq u_1 \leq 1, \quad 6.5 \leq u_2 \leq 7.5, \\ 82.1 \leq y_1 \leq 113.0, \quad 16.0 \leq y_2 \leq 18.0, \end{aligned} \tag{1}$$

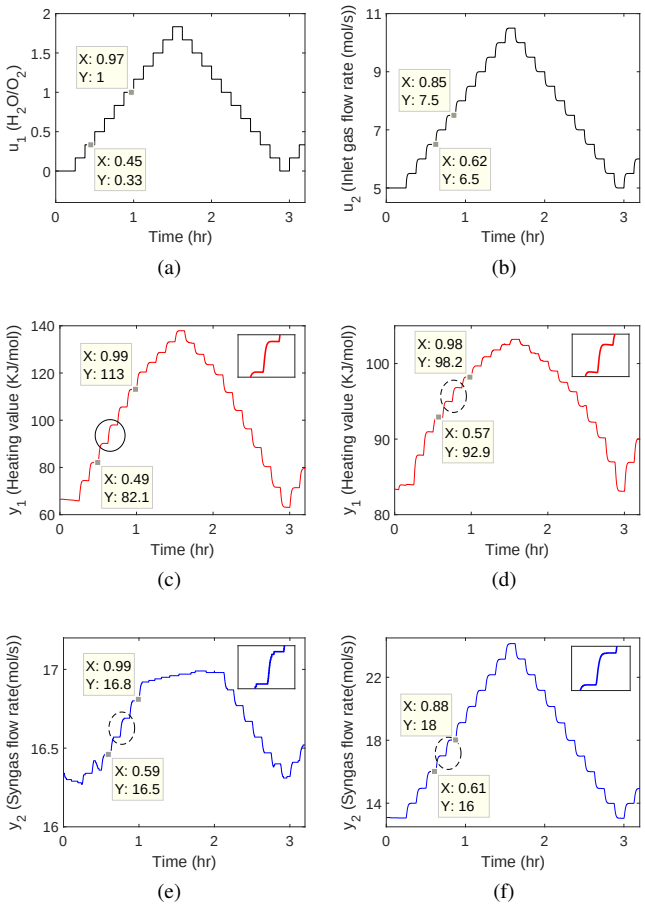

Fig. 1: UCG response for staircase inputs.

where u_1 (steam to oxygen ratio ($H_2O(g)/O_2(g)$)) and u_2 (inlet gas flow rate (mol/s)) represent inputs of the system. While y_1, y_2 are the outputs i.e. heating value (KJ/mol) and flow rate (mol/s) of syngas, respectively. The step responses of UCG are shown in Fig. 2, and it is found that there is no time delay between the input and output. The rise times and time constants determined by the step responses are summarized in Table I.

TABLE I: Parameters obtained from step response

Inputs	Outputs	Time constant (s)	Rise time (s)
u_1	y_1	20.83	34.5
	y_2	19.03	31.1
u_2	y_1	20.03	30.3
	y_2	21.04	31.6

B. Design of identification experiment

After acquiring the certain characteristics of model, the subsequent step is to conduct an experiment for the model estimation and validation. The most important part of identification experiment is the selection of an input signal, which must satisfy the property of persistent excitation i.e. its bandwidth should cover the range of all frequencies of interest [25], [29], [30]. The perturbed signals such as step, random binary

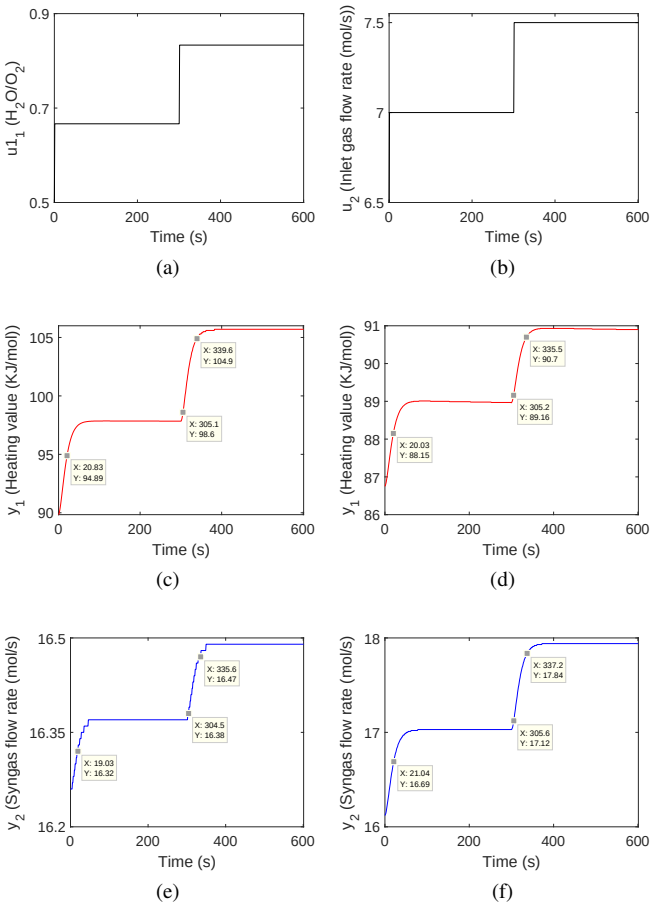

Fig. 2: Step response of UCG

sequence (RBS), pseudo random binary sequence (PRBS), white noise, multisine and swept sin (chirp) are typically used for the identification of unknown systems. These excitation signals have flat power spectrum band within the user specified frequency band. In [31], authors have shown that the construction of advanced dedicated signals is a challenging task, and the most commonly used signals for system identification are step and PRBS signals. In this work, PRBS signal has been used as an excitation signal and the design procedure is described in Table II.

A PRBS is a periodic signal, which switches in a certain fashion between two levels L_- and L_+, within a user specified frequency band. The bandwidth $[\omega_l \quad \omega_H]$ of input signal for multi-variable system is defined as

$$\omega_l = \frac{1}{\beta\tau_H} \leq \omega \leq \omega_H = \frac{\alpha}{\tau_l}, \tag{2}$$

where τ_H and τ_l are the highest and lowest time constants of the process, respectively, obtained from the step experiment; α is the ratio of open loop and desired closed loop time constants; $\beta\tau_H$ is the settling time of open loop system [29]. The number of shift registers (n_r) and the switching time T_{sw} are the important parameters to characterize the generated signal. The sequence repeats itself after $N_s T_{sw}$ units of time, where $N_s = 2^{n_r} - 1$. In [32], authors have presented the guidelines to choose the switching and sampling time of PRBS, and experiment length as

$$\frac{2.8\tau_l}{\alpha} \leq T_{sw} \leq \frac{2\pi\beta\tau_H}{N_s}, \tag{3}$$

$$N_s = 2^{n_r} - 1 = max\left(\frac{2\pi\beta\tau_H}{T_{sw}}, pD\right), \tag{4}$$

$$D = \frac{5\tau_H}{T_{sw}}, \quad t_s = T_{sw}/4,$$

where p is the number of inputs, t_s is the sampling time and D is the delay time. In MIMO system same PRBS can be used for all inputs provided that each input is delayed or shifted relative to the previous input by the delay time D in order to ensure that the input signals remain statistically uncorrelated. However, in this work separate PRBS is used for each input channel. The designed PRBS input signals having $T_{sw} = 27s$, $N_s = 15$ and maximum experiment length $N_s T_{sw} = 405$ samples, while the amplitude levels are defined on the basis of allowed linear operating range of each input.

C. Model estimation

The data de-trending has been performed as a pre-processing step to estimate the model. The system identification toolbox of MATLAB is used to identify the linear model. A number of different models like transfer function, state-space and process models are tried, and the best results are obtained from state-space model structure. The model is estimated by using N4SID estimation method. In the literature [33], [34], this approach has been discussed in detail and used to identify the model of batch processes. The model order is determined by evaluating a range of orders simultaneously. While the best order of the model is chosen from a Hankel singular value plot, as shown in Fig. 3. The plot indicates the relative contribution of each state to the input-output behavior of the model. It can be seen that the first two states have significant contribution. The red bar shows the over all best fit in minimizing the prediction error. The prediction error is a sum of the squares of the difference between the validation data output and the model output. Hence, a second order model is selected. The transfer functions are denoted by g_{ij}, where $i = 1,2$ represents the outputs and $j = 1,2$ denotes the corresponding inputs.

TABLE II: Parameters obtained from step response

Parameters		Values
Lowest dominating time constant	$\tau_l(s)$	20.03
Highest dominating time constant	$\tau_H(s)$	21.04
Number of inputs	p	2
Closed-loop response parameter	α	2
Settling-time parameter	β	3
Switching time	$T_{sw}(s)^*$	27
Delay time	$D(s)^*$	3.8
Number of bits in PRBS sequence of length $N_s = 2^{n_r} - 1$	n^{r*}	4

*Designed parameters, calculated from (3) and (4).

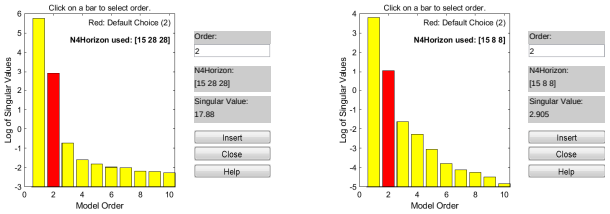

(a) g_{11}

(b) g_{12}

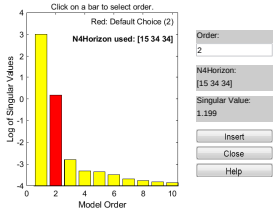

(c) g_{22}

Fig. 3: Hankel singular value plots for the selection of models order

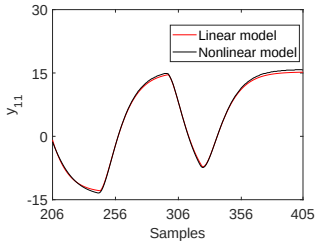

(a)

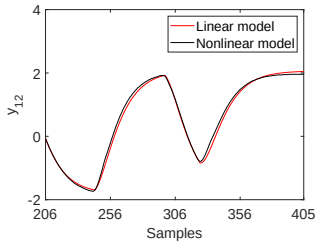

(b)

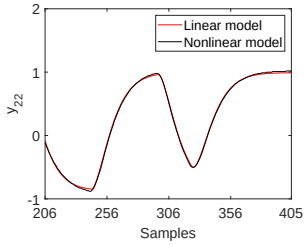

(c)

Fig. 4: Model validation using simulation method.

D. Model validation

The model has been validated by using the model simulation, residual analysis and prediction methods. The independent data sets for estimation and validation is obtained by splitting the data set into two parts. The first 205 samples of input-output data sets are used for model estimation and remaining 200 samples are used for model validation. The outputs of nonlinear and linear models for each input and output are compared in Fig. 4. The outputs are denoted by y_{ij}, where $i = 1,2$ represents the outputs and $j = 1,2$ denote the corresponding inputs. As it is found in preliminary experiments that u_1 has negligible impact on y_2, therefore, y_{21} has been ignored. It is found that the best fit results of each $y_{i,j}$ are 92.9%, 96.6% and 97.2%, respectively.

The residual analysis is an important part of system identification technique, which provides an insight about the model predictions [35]. It is essential that the residuals of each output must be uncorrelated with the past input signals in order to get better prediction results. In Fig. 5, it can be observed that the autocorrelation of residuals of each output and the cross-correlation between output residuals and each input lie within the confidence region. Moreover, the prediction method is used to determine the ability of identified models to forecast the future response of the system by using previous inputs and outputs. The 5-step ahead predicted outputs and errors are shown in Fig. 6. It is observed that the best Fit results of each model improved by 5.97%, 0.8 and 1.35% as compared to the simulation method. The prediction error methods is very much similar to the simulation error method except that, the true values of previous outputs are used to compute the error instead of the previous outputs predicted by the model. It is evident that the error in each model is small and in acceptable range. Moreover, these results can be improved by selecting the small prediction horizon.

The identified state-space models are converted into transfer functions. The transfer function form of all the identifies models are combined in a system matrix, and given as

$$\begin{bmatrix} y_1 \\ y_2 \end{bmatrix} = \begin{bmatrix} g_{11}(s) & g_{12}(s) \\ g_{21}(s) & g_{22}(s) \end{bmatrix} \begin{bmatrix} u_1 \\ u_2 \end{bmatrix}, \tag{5}$$

where g_{11}, g_{12} and g_{22} are given in Appendix A.

The system matrix is converted into state-space model with minimum realization of the system. Hence, the order of system matrix becomes 6. The resulting state-space model is given in (6) and (7)

$$\dot{\mathbf{x}} = A\mathbf{x} + B\mathbf{u}, \tag{6}$$

$$\mathbf{y} = C\mathbf{x}, \tag{7}$$

where $\mathbf{x} \in \Re^{n\times 1}$, $\mathbf{u} \in \Re^{m\times 1}$, $\mathbf{y} \in \Re^{p\times 1}$, $A \in \Re^{n\times n}$, $B \in \Re^{n\times m}$, $C \in \Re^{p\times n}$, and $n = 6, m = p = 2$. The scaled form of state-space matrices are given in Appendix A.

IV. Control Design

In this section, the linear model identified in (6) and (7) is employed to design a model-based multi-variable DSMC for the UPT field. The steps involved in the design of DSMC are briefly outlined below.

1) Plant scaling is performed as a preliminary step prior to the controller design for a multi-variable system.
2) The regular form is formulated to design the DSMC, and it is used to analyze the zero dynamics of the linear model.
3) The sliding variable vector $\mathbf{s} = \begin{bmatrix} s_1 & s_2 \end{bmatrix}$ is selected such that the sliding mode exhibits the desired properties.
4) The continuous part $\mathbf{u_{eq}}$ is computed by taking the time derivative of $\mathbf{s}$ and putting it equal to zero.
5) The discontinuous control is selected to enforce sliding mode by satisfying the condition: $\mathbf{s}\dot{\mathbf{s}} < 0$, which implies $\dot{\mathbf{u}}$ depends on discontinuous control.

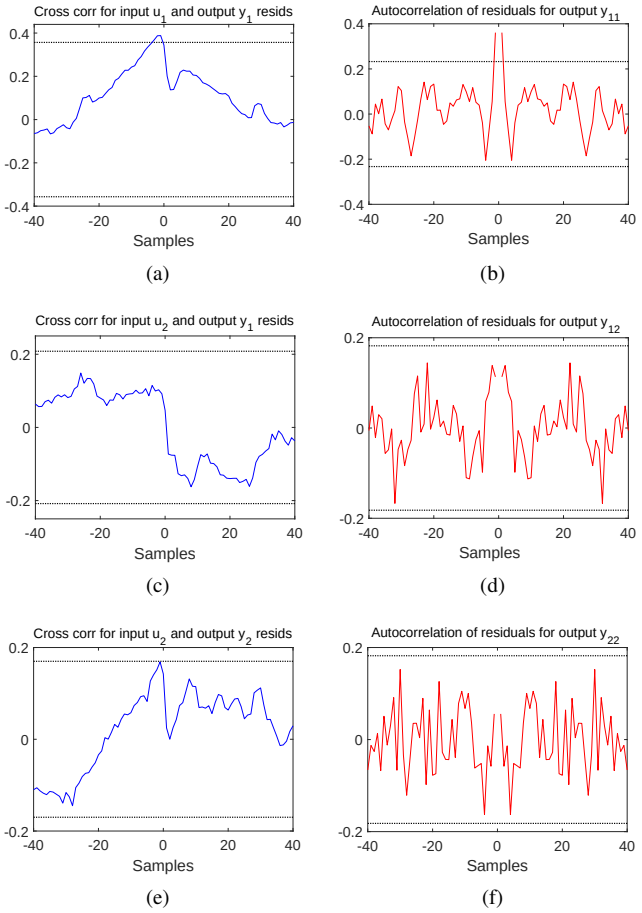

Fig. 5: Model validation using residual analysis.

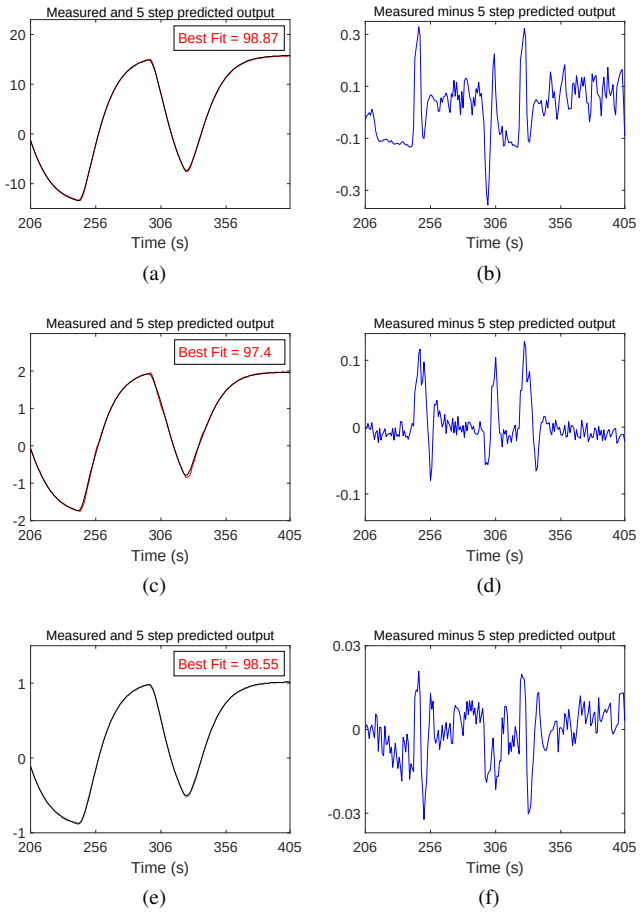

Fig. 6: Model validation using prediction method.

6) The zero dynamics of CAVSIM has been analyzed, and finally the DSMC is implemented on CAVSIM.

A. Plant scaling

Plant scaling is important in the multi-variable systems having different physical quantities. It helps the control engineer to make a decision about the desired performance of the system at the onset of controller design [36]. For this purpose, decision is made about the expected change in magnitudes of external signals like references, disturbance, measurement noise and maximum allowed deviation of each input and output around the nominal point. The unscaled linear model of the UCG system is given in (8).

$$\tilde{y} = \tilde{G}\tilde{u} + \tilde{G}_{d_i}\tilde{d}_i, \quad \tilde{e} = \tilde{y} - \tilde{r}, \tag{8}$$

where $(\tilde{.})$ is used to represent the variables in their actual unscaled units. The scaling is performed by dividing each variable with its maximum allowed variation around the nominal point. Let $\tilde{u}_{j,max}$, $\tilde{d}_{i,max}$, $\tilde{r}_{k,max}$ and $\tilde{e}_{k,max}$ denote the maximum allowed change in input $\tilde{u}_j$, input disturbance $\tilde{d}_i$, reference $\tilde{r}_k$ and control error $\tilde{e}_k$. As the variables $\tilde{y}$, $\tilde{r}$ and $\tilde{e}$ have the same units, therefore, same scaling factor i.e. maximum control error $(\tilde{e}_{max})$ is used for each of these variables. The unscaled and scaled quantities such as inputs, disturbances and control error are related by introducing the scaling matrices D_u, D_{d_i} and D_e, respectively.

$$\tilde{u} = D_u u, \quad \tilde{d}_i = D_{d_i} d_i, \quad \tilde{r} = D_e r, \quad \tilde{y} = D_e r. \tag{9}$$

The elements of scaling matrices are determined from (1), and are given as

$$D_u = \begin{bmatrix} 0.33 & 0 \\ 0 & 0.5 \end{bmatrix}, \; D_{d_i} = \begin{bmatrix} 0.33 & 0 \\ 0 & 0 \end{bmatrix}, \; D_e = \begin{bmatrix} 15 & 0 \\ 0 & 1 \end{bmatrix}. \tag{10}$$

B. Formulation of regular form

The eigenvalue placement problem in the framework of sliding mode control is solved by representing the linear system in a regular form, which makes the design simple [37]. The matrix B is partitioned by reordering the state vector components such as $B = \begin{bmatrix} B_1 \\ B_2 \end{bmatrix}$, where $B_1 \in \Re^{(n-m)\times m}$, $B_2 \in \Re^{m\times m}$ with $det\ B_2 \neq 0$ and $C = \begin{bmatrix} C_1 & C_2 \end{bmatrix}$, where $C_1 \in \Re^{(n\times m)-m}$, $C_2 \in \Re^{m\times m}$ with $det\ C_2 \neq 0$. The reordered states $(\mathbf{X})$ are decomposed into two vectors $\mathbf{X_1} = \begin{bmatrix} x_2 & x_3 & x_4 & x_6 \end{bmatrix}^T$ and $\mathbf{X_2} = \begin{bmatrix} x_1 & x_5 \end{bmatrix}^T$ such that (6), and (7) becomes

$$\dot{\mathbf{X}} = A\mathbf{X} + \begin{bmatrix} B_1 \\ B_2 \end{bmatrix} \mathbf{u}, \tag{11}$$

$$\mathbf{y} = C_1\mathbf{X_1} + C_2\mathbf{X_2}, \tag{12}$$

$$\mathbf{X_2} = C_2^{-1}(\mathbf{y} - C_1\mathbf{X_1}). \tag{13}$$

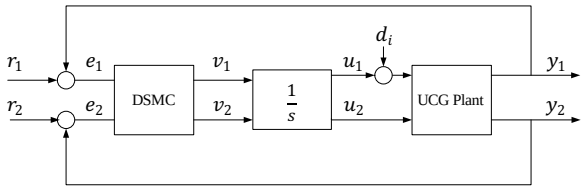

Fig. 7: Block Diagram of closed-loop UCG system with DSMC

By differentiating (12), and using (11) and (13), the matrix form of output and state vectors are represented by

$$\begin{bmatrix}\dot{\mathbf{X_1}}\\ \dot{\mathbf{y}}\end{bmatrix} = \begin{bmatrix}\alpha_{11} & \alpha_{12}\\ \alpha_{21} & \alpha_{22}\end{bmatrix}\begin{bmatrix}\mathbf{X_1}\\ \mathbf{y}\end{bmatrix} + \begin{bmatrix}B_1\\ CB\end{bmatrix}u, \tag{14}$$

where,

$$\begin{aligned}
&A = \left[\begin{array}{c|c} A_{11} & A_{12} \\ \hline A_{21} & A_{22}\end{array}\right], \quad \alpha = \left[\begin{array}{c|c} \alpha_{11} & \alpha_{12} \\ \hline \alpha_{21} & \alpha_{22}\end{array}\right],\\
&\alpha_{11} = \left[A_{11} - A_{12}C_2{}^{-1}C_1\right], \quad \alpha_{12} = \left[A_{12}C_2{}^{-1}\right],\\
&\alpha_{21} = \left[C_1A_{11} + C_2A_{21} - C_1A_{12}C_2^{-1}C_1 - C_2A_{22}C_2{}^{-1}C_1\right],\\
&\alpha_{22} = \left[C_1A_{12}C_2{}^{-1} + C_2A_{22}C_2{}^{-1}\right], \quad CB = C_1B_1 + C_2B_2.
\end{aligned}$$

The regular form is obtained by applying the nonsingular coordinate transformation T on (14).

$$\begin{aligned}
\begin{bmatrix}\mathbf{z}\\ \mathbf{y}\end{bmatrix} &= T\begin{bmatrix}\mathbf{X_1}\\ \mathbf{y}\end{bmatrix}, \quad T = \begin{bmatrix}I_{n-m} & -B_1(CB)^{-1}\\ O_{p\times(n-m)} & (CB)^{-1}\end{bmatrix}, \qquad (15)\\
\begin{bmatrix}\dot{\mathbf{z}}\\ \dot{\mathbf{y}}\end{bmatrix} &= T\alpha T^{-1}\begin{bmatrix}\mathbf{z}\\ \mathbf{y}\end{bmatrix} + T\begin{bmatrix}B_1\\ CB\end{bmatrix}\mathbf{u},\\
&= R\begin{bmatrix}\mathbf{z}\\ \mathbf{y}\end{bmatrix} + T\begin{bmatrix}B_1\\ CB\end{bmatrix}\mathbf{u},
\end{aligned}$$

where $R = T\alpha T^{-1}$, and the above equation can be expressed as

$$\begin{bmatrix}\dot{\mathbf{z}}\\ \dot{\mathbf{y}}\end{bmatrix} = \left[\begin{array}{c|c} R_{11} & R_{12} \\ \hline R_{21} & R_{22}\end{array}\right]\begin{bmatrix}\mathbf{z}\\ \mathbf{y}\end{bmatrix} + \begin{bmatrix}0\\ I\end{bmatrix}\mathbf{u}. \tag{16}$$

C. Design of DSMC

The conventional sliding mode control (SMC) is prone to chattering, which causes wear and tear of the actuators, reduces accuracy of the controller and excites the un-modeled dynamics. Therefore, in this work DSMC is employed to track the desired trajectories of heating value and flow rate of the syngas. In DSMC, sliding mode is enforced in the derivative of the control input, hence the control signal is continuous and chattering is reduced significantly. The overall DSMC control law is given as

$$\dot{\mathbf{u}} = \mathbf{v}, \tag{17}$$

where, $\mathbf{v}$ is to be selected. The sliding variable vector ($\mathbf{s}$) is selected to maintain the heating value and flow rate of syngas at the desired levels ($\mathbf{y_d} = \begin{bmatrix}y_{d_1} & y_{d_2}\end{bmatrix}^T$). The desired objectives should be achieved when $\mathbf{s} \to 0$, therefore,

$$\mathbf{s} = \dot{\mathbf{e}} + \kappa_1\mathbf{e}, \quad \text{and} \quad \mathbf{e} = \mathbf{y} - \mathbf{y_d}. \tag{18}$$

Now the control input vector $\mathbf{v}$ is obtained by taking the time derivative of $\mathbf{s}$ as

$$\begin{aligned}
\dot{\mathbf{s}} &= \ddot{\mathbf{e}} + \kappa_1\dot{\mathbf{e}},\\
&= \Theta_1\mathbf{z} + \Theta_2\mathbf{y} + \Theta_3\mathbf{u} + \Theta_4 + \mathbf{v}, \qquad (19)
\end{aligned}$$

where $\Theta_1 = R_{21}R_{11} + R_{22}R_{21} + \kappa_1R_{21}$, $\Theta_2 = R_{21}R_{12} + R_{22}^2 + \kappa_1R_{22}$, $\Theta_3 = R_{22} + \kappa_1$ and $\Theta_4 = -\ddot{\mathbf{y}}_\mathbf{d} - \kappa_1\dot{\mathbf{y}}_\mathbf{d}$. While κ_1 is a positive definite diagonal matrix.

By selecting $\mathbf{v} = -\Theta_1\mathbf{z} - \Theta_2\mathbf{y} - \Theta_3\mathbf{u} - \Theta_4 - Nsign(\mathbf{s})$, (19) becomes

$$\dot{\mathbf{s}} = -Nsign(\mathbf{s}), \tag{20}$$

where, $N = \begin{bmatrix}N_1 & 0\\ 0 & N_2\end{bmatrix}$ and $N_1 \in \Re^+$, $N_2 \in \Re^+$. As $\mathbf{s}^T\dot{\mathbf{s}} = -N|\mathbf{s}| < 0$, hence, the sliding mode exists and the over all control-law is

$$\dot{\mathbf{u}} = \mathbf{v} = -Nsign(\mathbf{s}) - \Theta_1\mathbf{z} - \Theta_2\mathbf{y} - \Theta_3\mathbf{u} - \Theta_4. \tag{21}$$

The control input vector $\mathbf{u}$ is obtained after integrating (21), as shown in Fig. 7. The internal dynamics from (16) is given as

$$\dot{\mathbf{z}} = R_{11}\mathbf{z} + R_{12}\mathbf{y}, \tag{22}$$

$$\tag{23}$$

When the sliding mode is established i.e $\mathbf{s} = 0$, then, with positive definite diagonal matrix κ_1, the tracking error vector given by (19) converges to the origin asymptotically, which implies $\mathbf{y} \to \mathbf{y_d}$. The matrix R_{11} in (22) is shown in Appendix A. The matrix R_{11} is Hurwitz which shows that the zero dynamics is stable. The boundedness of states show that $\mathbf{v}$ is also bounded, as Θ_3 in (17) is Hurwitz and outputs are also bounded. As the zero dynamics and the control inputs are bounded, therefore, the design of DSMC is valid.

V. Approximate Model of CAVSIM

The stability and tracking objective of the linear system have been achieved by using the control design given in (21). Now, it is desired to implement the controller on the actual CAVSIM and to prove the stability of the zero dynamics of CAVSIM. Due to the complex dynamics of the CAVSIM model, the 1D packed model of [19] is used to approximate CAVSIM. The fundamental dynamics of both the models are based on the laws of mass and energy conservations of solids and gases. However, the model of [19] is simpler but less accurate. In order to prove the stability of the zero dynamics the model of [19] is modified by incorporating the expression for the flow rate of the produced gas (y_2).

A. Model Equations

The model comprises of two solids coal and char, and eight gases: $CO, CH_4, H_2, CO_2, H_2O(g), N_2, O_2$ and C_nH_m. The model is simplified by considering only the coal pyrolysis, char oxidation, and steam gasification reactions [20], and the reaction rates are given in (27), (28) and (29). The coal density (ρ_1), char density (ρ_2) and solid temperature (T_s) are states of the UCG system, and given by the following PDEs [21]. The

following equations are based on the laws of conservation of mass and energy for coal and char. The definition and symbols of model parameters is given in Table III.

$$\frac{\partial \rho_1}{\partial t} = -M_1 R_1, \tag{24}$$
$$\rho_1(0,x) = \rho_{1_0}(x), \quad 0 \le x \le L.$$
$$\frac{\partial \rho_2}{\partial t} = M_2\left[|a_{s_{2,1}}|R_1 - R_2(u) - R_3(u)\right], \tag{25}$$
$$\rho_2(0,x) = \rho_{2_0}(x), \quad 0 \le x \le L.$$
$$\frac{\partial T_s}{\partial t} = \frac{B\dfrac{\partial^2 T_s}{\partial x^2} + h(T_o - T_s) - q_1 R_1 - q_2 R_2(u) - q_3 R_3(u)}{(cp_1\rho_1 + cp_2\rho_2)}, \tag{26}$$
$$T_s(0,x) = T_{s_0}(x), \quad 0 \le x \le L,$$
$$\frac{\partial T_s}{\partial x}(t,0) = \frac{\partial T_s}{\partial x}(t,L) = 0, \quad t \ge 0,$$

where,

$$R_1 = 5\frac{\rho_1}{M_1}\exp\left(\frac{-6039}{T_s}\right), \tag{27}$$
$$R_2 = f_{R_2}(u_1,u_2)R_{C_2}, \tag{28}$$
$$f_{R_2}(u_1,u_2) = \frac{1}{u_1+u_2},$$
$$R_{C_2} = \frac{9.55\times10^8\rho_2 P v_g C_7 \exp\left(\dfrac{-22142}{T_s}\right)k_y}{M_2 k_y\sqrt{T_s} + 9.55\times10^8\rho_2 P\exp\left(\dfrac{-22142}{T_s}\right)},$$
$$C_7 = 0.21\frac{u_2}{v_g}\exp\left(-\frac{|a_{7,2}|}{u_1+u_2}\int_0^x R_{C_2}dx\right),$$
$$R_3 = f_1(u_1,u_2)R_{C_3}, \tag{29}$$
$$f_1(u_1,u_2) = \frac{u_1}{u_1+u_2},$$
$$R_{C_3} = \frac{k_y P^2\rho_2 E_1}{P^2E_1\rho_2 + k_y M_2(P+E_2)^2},$$
$$E_1 = \exp\left(5.052 - \frac{12908}{T_s}\right),$$
$$E_2 = \exp\left(-22.216 + \frac{24880}{T_s}\right).$$

The syngas collected at the production well is sent to the gas analyzer which provides the molar fraction and flow rate of syngas species. The two outputs i.e. the heating value and flow rate of syngas are calculated as

$$y_1 = m_1H_1 + m_2H_2 + m_3H_3 + m_4H_4, \tag{30}$$
$$m_i = 100\frac{C_i(L)}{\tilde{C_T}(L)}, \tilde{C_T}(L) = \sum_{i=1,i\neq4}^{8} C_i(L),$$
$$y_2 = \tilde{C_T}v_g, \tag{31}$$

where y_i with $i = 1,2$ represents the outputs (heating value and flow rate of syngas), H_i and m_i are the heat of combustion, molar fraction percentage of syngas species CO, CH_4, H_2 and C_nH_m and total concentration of syngas, respectively. While

TABLE III: List of symbols

Symbol	Description
ρ_i	Solid density (g/cm^3), $i = 1,2$ for coal and char
M_i	Molecular weight (g/mol), $i = 1,2$ for coal and char
$a_{s_{2,1}}$	Stoichiometric coefficient of char in coal pyrolysis reaction
T_s, T_o	Solid and gas temperatures (K)
B	A constant depending on the coal bed porosity and thermal conductivity of coal and char (cal/cm/s/K)
h	Heat transfer coefficient (cal/s/K/cm^3)
q_i	Heat of reaction i (cal/mol)
c_{p_i}	Heat capacity (cal/g/K), $i = 1$ for coal and $i = 2$ for char
R_i	Rate of a chemical reaction (mol/cm^3/s), $i = 1,2,3$ represents pyrolysis, char oxidation and steam gasification respectively
$a_{i,j}$	Stoichiometric coefficient of gas i in reaction j
H_i	Heat of combustion (kJ/m^3) of gas, $i = 1,3,5,8$ represents CO, H_2, CH_4 and tar
t, x	Variables for time (s) and length (cm)
C_7	Distribution of O_2 concentration (mol/cm^3) along x
P, v_g	Pressure (atm) and velocity (cm/s) of gases
k_y	Mass transfer coefficient (mol/cm^3/s)
L	Length of the reactor: $2500cm$

$\tilde{C_T}$ and v_g represent the concentration and velocity of syngas. The mass balance of gases is given by [19]

$$\frac{dC_i}{dx} = \frac{1}{v_g}\left(-C_i\frac{dv_g}{dx} + \sum_{j=1}^{3} a_{ij}R_j\right),$$

where R_j represent the reaction rates given in (27), (28) and (29). The solution for CO, CH_4, H_2, CO_2 and C_nH_m at $x = L$ with $C_i(0) = 0$ is [21]

$$C_i(L) = \frac{1}{v_g}\sum_{j=1}^{3} a_{i,j}\int_0^L R_j dx. \tag{32}$$

O_2 contributes only in char oxidation reaction and N_2 is an inert gas and it does not participate in any chemical reaction. Therefore, the solution for the concentration of O_2 $C_{O_2}(L)$, with $C_{O_2}(0) = 0.21\dfrac{u_2}{v_g}$ and N_2 is

$$\frac{dC_{O_2}}{dx} = -\frac{|a_{7,2}|}{v_g}R_2,$$
$$C_{O_2}(L) = 0.21\frac{u_2}{v_g}\exp\left(-\frac{|a_{7,2}|}{u_1+u_2}\int_0^L CR_2\right), \tag{33}$$
$$C_{N_2}(L) = C_{N_2}(0) = \frac{1}{v_g}(0.79u_2 - 0.21u_1u_2). \tag{34}$$

Hence, (30) and (31) become

$$y_1 = \frac{N_1 + f_1(u_1,u_2)N_2}{D1 + f_1(u_1,u_2)D_2 + f_2(u_1,u_2)}, \quad (35)$$

$$y_2 = D1 + f_1(u_1,u_2)D_2 + f_2(u_1,u_2), \quad (36)$$

where, $f_1(u_1,u_2) = \dfrac{u_1}{u_1+u_2}$,

$$f_2(u_1,u_2) = \frac{0.79u_2 - 0.21u_1u_2}{v_g},$$

$$N_1 = 100\alpha \int_0^L R_1 dx,$$

$$N_2 = 100\beta \int_0^L R_{C3} dx,$$

$$D_1 = \gamma \int_0^L R_1 dx + \zeta \int_0^L R_2 dx,$$

$$D_2 = +\eta \int_0^L R_{C3} dx,$$

$$f_2(u_1,u_2) = \frac{1}{v_g}\left(0.79u_2 - 0.21u_1u_2\right),$$

$$\alpha = \frac{1}{v_g}\left(a_{11}H_1 + a_{31}H_3 + a_{51}H_5 + a_{81}H_8\right),$$

$$\beta = \frac{1}{v_g}\left(a_{13}H_1 + a_{33}H_3\right),$$

$$\gamma = \frac{1}{v_g}\left(a_{11} + a_{21} + a_{31} + a_{51} + a_{81}\right),$$

$$\eta = \frac{1}{v_g}\left(a_{13} + a_{33}\right),\ \zeta = \frac{a_{2,2}}{v_g}.$$

B. Stability of zero dynamics of CAVSIM

As the DSMC in (21) tracks y_1 and y_2 to the desired trajectories given by $\mathbf{y_d}$. Now it is essential to determine the stability of the zero dynamics for CAVSIM. It is evident from (35) and (36) that both the outputs are directly dependent on control inputs u_1 and u_2, hence the relative degree of the system is 0. Therefore, all the solid PDEs given in (24)-(26) constitute the zero dynamics of the system with $u = u_{DSMC}$ which makes $\mathbf{s} = 0$ at $t = t_{ss}$. The states are stable iff the reaction rates and control inputs are bounded. While the reaction rates in (27), (28) and (29) are the functions of control inputs u_1, u_2, solid gas temperature T_s and the densities of coal and char (ρ_1, ρ_2). The solution of (24) is given as [21]

$$\rho_1(t,x) = \rho_1(0,x)\exp(-5E_3 t), \quad (37)$$

$$E_3(x) \le \exp\left\{\frac{-6039}{\max\limits_{t\ge 0} T_s(t,x)}\right\}, \quad 0 < T_{smin} \le T_s(t,x).$$

It is important to note that for $0 < T_{smin} \le T_s(t,x) \le \infty$, the distribution $\rho_1(0,x)$ exponentially decays with time, and ρ_1 is stable. The stability of ρ_2 can also be inferred from the stability of ρ_1, because ρ_1 is decomposed by coal pyrolysis reaction to yield ρ_2 and product gases, therefore, for law of conservation of mass to hold, ρ_2 is bounded [21].

According to [21], the heat equation in (26) can be approximated with the following linear PDE as

$$\dot{T}_s = \frac{1}{\bar{C}_s}\left[BT_s'' - hT_s + hT(x) + \mathscr{G}(t,x)\right], \quad (38)$$

$$|\mathscr{G}(t,x)| \le \mathscr{G}_0,\ \mathscr{G}_0 \in \Re^+,$$

where $\dot{T}_s = \dfrac{\partial T_s}{\partial t}$, $T_s' = \dfrac{\partial T_s}{\partial x}$, $T_s'' = \dfrac{\partial^2 T_s}{\partial x^2}$ and $\mathscr{G}(t,x)$ is a linear function and an upper bound on the heat source term (H_s). The solution of above equation can be represented as

$$T_s = \Delta T_s + T_{sx} + T_{sd}, \quad (39)$$

where, ΔT_s corresponds to the solution without the inputs $T(x)$ and $\mathscr{G}$, T_{sx} is the forced component defined by $T(x)$ and T_{sd} is the forced part which depends on the disturbance $\mathscr{G}(t,x)$. Now the boundedness of all the solution components in (39) is investigated independently. The stability of homogeneous equation is given as

$$\bar{C}_s\Delta\dot{T}_s = B\Delta T_s'' - h\Delta T_s,$$
$$\Delta T_s(0,x) = \Delta T_{s_0}(x),\ \Delta T_s'(t,0) = \Delta T_s'(t,L) = 0.$$

By selecting a positive definite Lyapunov functional as

$$V = \frac{\bar{C}_s}{2}\int_0^L \Delta T_s^2 dx > 0 \quad if\ s \ne 0.$$

Then taking its time derivative

$$\dot{V} = B\int_0^L \Delta T_s \Delta T_s'' dx - h\int_0^L \Delta T_s^2 dx,$$
$$= -B\int_0^L \Delta T_s'^2 dx - \frac{2h}{\bar{C}_s}V.$$

Now using Poincare Inequality: for any continuously differentiable ΔT_s on $[0,L]$

$$\int_0^L \Delta T_s^2 dx \le 2\Delta T_s^2(L) + 4\int_0^L \Delta T_s'^2 dx.$$

After using $\Delta T_s'(t,L) = 0 \implies \frac{1}{2}\Delta T_s^2(L) = \Omega \in \Re^+$. The expression for $\dot{V}$ becomes

$$\dot{V} \le -\alpha V + \Omega,$$
$$V \le \frac{\Omega}{\alpha}\Big(1 - exp(-\alpha t)\Big),$$
$$\alpha = 2\frac{B+h}{\bar{C}_s}.$$

The $L-2$ norm of ΔT_s is defined as

$$||\Delta T_s(t)|| = \left(\int_0^L \Delta T_s(t,x)^2 dx\right).$$

Therefore, $L-2$ norm of ΔT_s is bounded and given by

$$||\Delta T_s(t)|| \le -\zeta\left(1 - \exp\Big(\frac{-\alpha}{2}t\Big)\right) + ||\Delta T_{s_0}||\exp\Big(\frac{-\alpha}{2}t\Big),$$

$$\zeta = \sqrt{\frac{2\Omega}{\alpha\bar{C}_s}}, \quad \Delta T_{s_0}(x) = \Delta T_s(0,x).$$

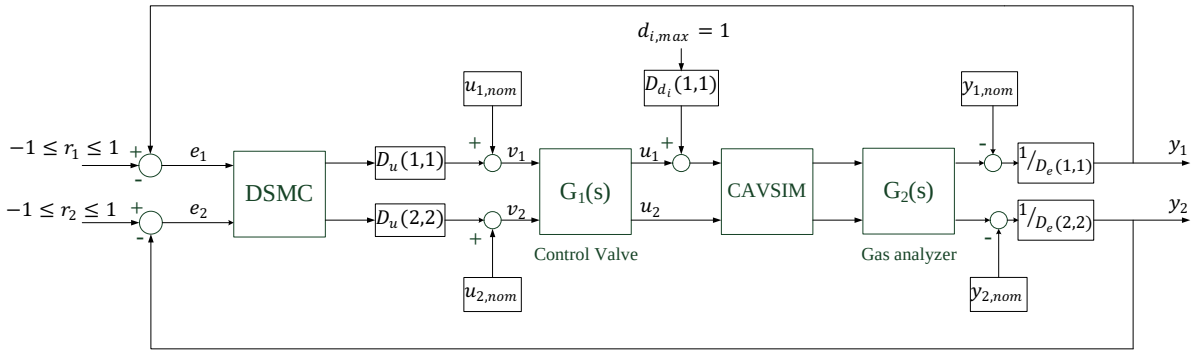

Fig. 8: Implementation of DSMC on CAVSIM

The following boundary value problem is solved to obtain T_{sx}

$$BT_{sx}'' - hT_{sx} + hT(x) = 0,$$
$$T_{sx}'(t,0) = T_{sx}'(t,L) = 0,$$
$$T(x) = T(0)\exp(-\lambda x) + \lambda \int_0^x \exp\{-\lambda(x-\mathscr{X})\} T_s(\mathscr{X}) d\mathscr{X}.$$

Eventually the solution is [21]

$$T_{sx} = -\frac{\Lambda}{\lambda^2 B - h}\exp(-\lambda x), \tag{40}$$
$$\lambda = \frac{h}{v_g C_g},$$
$$\Lambda = h\left[T(0) + T_s(0,0)\right].$$

Therefore, the forced response T_{sx} due to $T(x)$ is also bounded. As the disturbance $\mathscr{G}$ in the linear approximation of heat source term, therefore, T_{sd} is also bounded. The boundedness of T_{sd} can be shown if it is represented in the modal form. All the solution components of the linear heat equation are bounded, therefore, T_s stays bounded throughout the process of gasification. As described in section IV-C that $\mathbf{u}$ is bounded, the results in (37) and the boundedness of T_s show that the zero dynamics of the UCG process is bounded and the design of DSMC is valid.

VI. Implementation of DSMC on CAVSIM

As the controller design is based on a very simple linear model given in (6) and (7), while the CAVSIM is highly complex, therefore, it is essential to implement the designed controller on CAVSIM in order to assess the robustness and performance of DSMC. The CAVSIM computer code has been developed by LLNL, and it is written in FORTRAN and a Microsoft Developer Studio is used to run the program [38].

The implementation of designed controller on CAVSIM is a challenging task, and it requires detailed understanding of the 3D model and the computer code. The model mechanistically calculates cavity surface recession rates from mass and energy balances, and it is capable to simulate the cavity growth for entire life of UCG. It also integrates the results of different but interacting submodels, describing dispersion of injected reactants in a rubble bed at the bottom of cavity, water influx from the coal aquifer, degradation of rubble-covered coal sidewalls due to thermal stress and chemical reactions, recession of cavity surfaces enclosing a void space in the upper cavity caused by radiation-driven spalling and gasification, and calculates the growth of outflow channel.

The dynamics of control valve and gas analyzer have been included in CAVSIM with the following transfer functions, respectively [21].

$$G_1(s) = \frac{1}{\tau_c s + 1}, \quad G_2(s) = \frac{1}{\tau_g s + 1}. \tag{41}$$

It has been experimentally found that $\tau_c = \tau_g = 10s$. The implementation scheme of DSMC on actual system is shown in Fig. 8. It is pertinent to mention that the controller has been designed from a scaled model, therefore, the scaling matrices (D_u, D_e, D_{d_i}) given in (10) are essential to be included in the implementation scheme of the designed controller. Moreover, the nominal operating points of inputs are included after the inputs scaling matrix in such a way that the inputs fed to CAVSIM are the actual inputs. While in order to create the scaled inputs to the controller, the nominal operating points of outputs are subtracted from the actual outputs of CAVSIM prior to output scaling matrix and feedback.

As described in section IV-B , the nonsingular coordinate transformation T in (15) is applied on the actual system to design the continuous part of the controller. Thus, the inverse transformation is applied to obtain the controller in terms of actual states $\mathbf{X_1}$ and $\mathbf{X_2}$.

$$\mathbf{v} = -Nsign(\mathbf{s}) - \Delta\begin{bmatrix}\mathbf{X_1}\\ \mathbf{y}\end{bmatrix} - \Theta_3\mathbf{u} - \Theta_4,$$
$$\text{where,} \quad \Delta = \begin{bmatrix}\Theta_1 & \Theta_2\end{bmatrix} T = \left[\begin{array}{c:c} -\frac{\Delta_{11}}{\Delta_{21}} & \frac{\Delta_{12}}{\Delta_{22}} \end{array}\right].$$

By using (12), the over-all control becomes

$$\mathbf{v} = -N_1 sign(\mathbf{s}) - \Gamma\begin{bmatrix}\mathbf{X_1}\\ \mathbf{X_2}\end{bmatrix} - \Theta_3\mathbf{u} - \Theta_4, \tag{42}$$

where,

$$\Gamma = \left[\begin{array}{c:c} -\frac{\Delta_{11}+\Delta_{12}C_1}{\Delta_{21}+\Delta_{22}C_1} & \frac{\Delta_{12}C_2}{\Delta_{22}C_2} \end{array}\right].$$

Moreover, the time derivative of the tracking error, required in the sliding variable equation (18) is given as

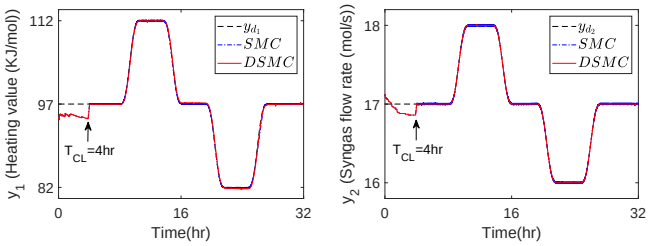

(a) (b)

Fig. 9: Outputs of the closed-loop system with time.

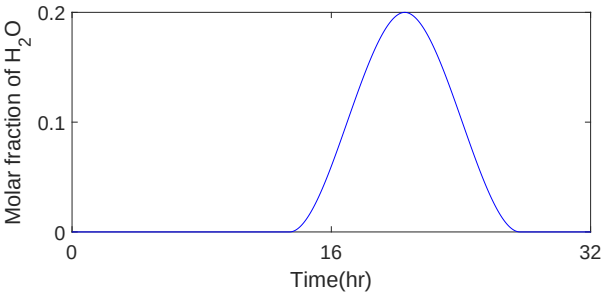

Fig. 11: Input disturbance with time

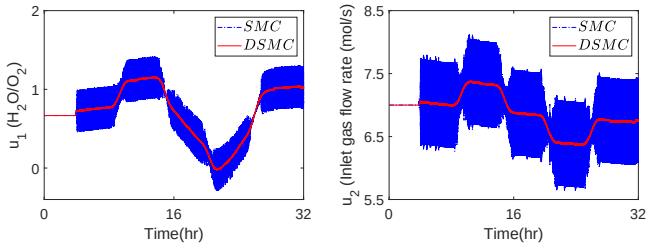

(a) (b)

Fig. 10: Control efforts with time.

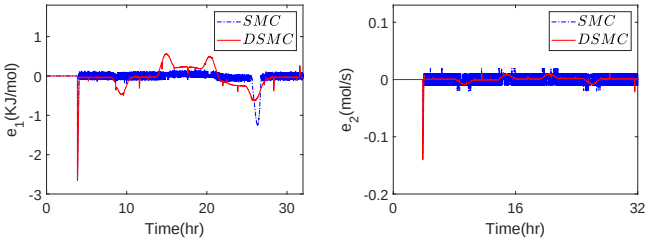

(a) (b)

Fig. 12: Tracking errors during closed-loop operation.

$$\dot{\mathbf{e}} = \begin{bmatrix}\Phi_1 & \Phi_2\end{bmatrix}\mathbf{X} + \Phi_3\mathbf{u} - \dot{\mathbf{y}}_\mathbf{d}, \tag{43}$$

where, $\Phi_1 = \left[C_1A_{11} + C_2A_{21}\right]$,

$\Phi_2 = \left[C1A_{12} + C_2A_{22}\right]$,

$\Phi_3 = \left[C_1B_1 + C_2B_2\right]$.

The control law is implemented by employing a finite difference method on (42) and (43), and the discretized controller is given as

$$\mathbf{u}(k) = \mathbf{u}(k-1) + dt(-N_1 sign(\mathbf{s}) - \Gamma\begin{bmatrix}\mathbf{X_1}\\ \mathbf{X_2}\end{bmatrix} - \Theta_3\mathbf{u} - \Theta_4), \tag{44}$$

where, Γ, Θ_3 and Θ_4 are given in Appendix A.

VII. Results and Discussions

In this section, the performance of DSMC on CAVSIM has been shown, and simulation results are discussed. Moreover, a comparison is made between the DSMC and conventional SMC. Initially, the simulation runs in open loop configuration with the nominal inputs and the controller begins operation at 04^{th} hour. Ideally, the controller should maximize the energy output per unit time by keeping both the outputs at their maximum allowed values. However, the peak values of heating value and flow rate drop due to the growth of cavity in UCG reactor. In Fig. 9, the desired trajectories of outputs are chosen in such a way that they cover the complete operating range, as identified in (1). It has been observed that both the controllers have achieved the tracking objectives in the presence of input disturbance and modeling uncertainties. The control inputs are shown in Fig. 10, and it is evident that the DSMC has achieved the desired control objective by consuming less control effort as compared to SMC. The chattering is prominent for the SMC, whereas in case of DSMC the chattering is significantly reduced due to continuous control inputs.

Moreover, the capability of DSMC to reject the disturbance is assessed by introducing an input disturbance around the 14^{th} hour, as shown in Fig. 11. In UCG an optimal level of H_2O is required for the successful operation, while an excess water influx from surrounding strata reduces the temperature of a UCG reactor and disrupts its operation. The increase in water favors the endothermic steam gasification reaction and decreases the temperature of UCG rector. Therefore, water influx from surrounding strata is considered as an input disturbance, as it increases the $H_2O(g)/O_2(g)$. It can be seen in Fig. 10a that the controller maintains an optimal amount of H_2O by varying $H_2O(g)/O_2(g)$. Thus, the designed DSMC exhibits adequate performance and robustness against the model inaccuracies and an input disturbance, as shown in Fig. 9. The corresponding tracking errors during the closed-loop operation are shown in Fig. 12. The time profile of sliding variable vector $\mathbf{s}$ given in (18) is shown in Fig. 13. It is observed that the sliding manifolds and errors remain in the close proximity of zero during the time when the controller is brought into operation.

VIII. Conclusion

In this manuscript, it has been shown that the multi-variable closed-loop system is important for increasing the energy output per unit time and hence efficiency of the UCG field. The actual UCG model is highly complex; it is not possible to use this model for the model-based control design. A multi-variable linear model has been formulated by using N4SID system identification technique to design a DSMC for the UPT field. Moreover, an approximated 1D model is

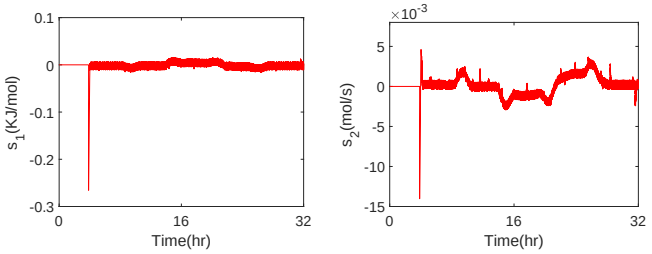

(a) (b)

Fig. 13: Sliding manifolds for DSMC.

also formulated for the MIMO CAVSIM, and it has been shown that the zero dynamics of the model are stable with the designed controller. Eventually, the designed controller is implemented on the CAVSIM. The simulation results of DSMC have been compared with conventional SMC, which show that both the controllers track the desired trajectories. However, DSMC utilizes lesser control energy to achieve the desired objectives. As the control inputs are continuous in case of DSMC, therefore, the chattering is also reduced.

APPENDIX

$$g_{11}(s)=\frac{1.79s+1.45}{s^2+0.2s+0.01},\quad g_{12}(s)=\frac{0.0465s+0.0347}{s^2+0.191s+0.00897},$$
$$g_{21}(s)=0,\qquad g_{22}(s)=\frac{0.01951s+0.0199}{s^2+0.1993s+0.01071}.$$

$$A=\begin{bmatrix}-0.2 & -0.08 & 0 & 0 & 0 & 0\\ 0.12 & 0 & 0 & 0 & 0 & 0\\ 0 & 0 & -0.19 & -0.07 & 0 & 0\\ 0 & 0 & 0.12 & 0 & 0 & 0\\ 0 & 0 & 0 & 0 & -0.20 & -0.08\\ 0 & 0 & 0 & 0 & 0.12 & 0\end{bmatrix},$$

$$B=\begin{bmatrix}0.25 & 0\\ 0 & 0\\ 0 & 0.12\\ 0 & 0\\ 0 & 0.5\\ 0 & 0\end{bmatrix},C=\begin{bmatrix}0.06 & 0\\ 0.39 & 0\\ 0.02 & 0\\ 0.13 & 0\\ 0 & 0.027\\ 0 & 0.22\end{bmatrix}^T.$$

$$R_{11}=\begin{bmatrix}-0.81 & -0.04 & -0.27 & 0\\ 0 & -0.19 & -0.07 & 1.69\\ 0 & 0.12 & 0 & 0\\ 0 & 0 & 0 & -1.02\end{bmatrix}.$$

$$\Gamma=\begin{bmatrix}-0.23 & -0.09 & -0.07 & 0.03 & -0.28 & 0.03\\ 0 & 0 & 0 & -0.16 & 0 & -0.18\end{bmatrix},$$

$$\Theta_3=\begin{bmatrix}0.71 & -0.05\\ 0 & 0.92\end{bmatrix},$$

$$\Theta_4=\begin{bmatrix}-1 & 0 & -0.1 & 0\\ 0 & -1 & 0 & -0.1\end{bmatrix}\begin{bmatrix}\ddot{y}_{d_1} & \ddot{y}_{d_2} & \dot{y}_{d_1} & \dot{y}_{d_2}\end{bmatrix}^T.$$

REFERENCES

[1] I. E. Agency, *World Energy Outlook 2019*. OECD Publishing, Paris, 2019.

[2] G. Perkins, "Underground coal gasification–part i: Field demonstrations and process performance," *Progress in Energy and Combustion Science*, vol. 67, pp. 158–187, 2018.

[3] ——, "Underground coal gasification–part ii: Fundamental phenomena and modeling," *Progress in Energy and Combustion Science*, vol. 67, pp. 234–274, 2018.

[4] R. Sathre, L. Gustavsson, and N. Le Truong, "Climate effects of electricity production fuelled by coal, forest slash and municipal solid waste with and without carbon capture," *Energy*, vol. 122, pp. 711–723, 2017.

[5] A. W. Bhutto, A. A. Bazmi, and G. Zahedi, "Underground coal gasification: From fundamentals to applications," *Progress in Energy and Combustion Science*, vol. 39, no. 1, pp. 189–214, 2013.

[6] G. Perkins, "Mathematical modeling of underground coal gasification," Ph.D. dissertation, PhD Thesis: School of Materials Science & Engineering, Faculty of Science …, 2005.

[7] A. A. Uppal, "Modeling and control of underground coal gasification," Ph.D. dissertation, COMSATS Institute of Information Technology, Islamabad, Pakistan, 2016.

[8] S. B. Javed, A. A. Uppal, A. I. Bhatti, and R. Samar, "Prediction and parametric analysis of cavity growth for the underground coal gasification project thar," *Energy*, vol. 172, pp. 1277–1290, 2019.

[9] A. Arshad, A. I. Bhatti, R. Samar, Q. Ahmed, and E. Aamir, "Model development of ucg and calorific value maintenance via sliding mode control," in *2012 International Conference on Emerging Technologies*. IEEE, 2012, pp. 1–6.

[10] G. Samdani, P. Aghalayam, A. Ganesh, and S. Mahajani, "A process model for underground coal gasification–part-iii: Parametric studies and ucg process performance," *Fuel*, vol. 234, pp. 392–405, 2018.

[11] K. Kostúr and J. Kacur, "Development of control and monitoring system of ucg by promotic," in *2011 12th international carpathian control conference (ICCC)*. IEEE, 2011, pp. 215–219.

[12] K. Kostúr and J. Kačúr, "The monitoring and control of underground coal gasification in laboratory conditions," *Acta Montanistica Slovaca*, vol. 13, no. 1, pp. 111–117, 2008.

[13] K. J. Åström and T. Hägglund, *PID controllers: theory, design, and tuning*. Instrument society of America Research Triangle Park, NC, 1995, vol. 2.

[14] K. Kostúr and J. Kačur, "Extremum seeking control of carbon monoxide concentration in underground coal gasification," *IFAC-PapersOnLine*, vol. 50, no. 1, pp. 13 772–13 777, 2017.

[15] J. Kacur, P. Flegner, M. Durdán, and M. Laciak, "Model predictive control of ucg: An experiment and simulation study," *Information Technology and Control*, vol. 48, no. 4, pp. 557–578, 2019.

[16] D. W. Camp, "A review of underground coal gasification research and development in the united states," Lawrence Livermore National Laboratory (LLNL), California, USA, Tech. Rep. LLNL-TR-733952, 2017.

[17] A. A. Uppal, S. S. Butt, A. I. Bhatti, and H. Aschemann, "Integral sliding mode control and gain-scheduled modified utkin observer for an underground coal gasification energy conversion process," in *2018 23rd International Conference on Methods & Models in Automation & Robotics (MMAR)*. IEEE, 2018, pp. 357–362.

[18] A. A. Uppal, S. S. Butt, Q. Khan, and H. Aschemann, "Robust tracking of the heating value in an underground coal gasification process using dynamic integral sliding mode control and a gain-scheduled modified utkin observer," *Journal of Process Control*, vol. 73, pp. 113–122, 2019.

[19] A. A. Uppal, A. I. Bhatti, E. Aamir, R. Samar, and S. A. Khan, "Control oriented modeling and optimization of one dimensional packed bed model of underground coal gasification," *Journal of Process Control*, vol. 24, no. 1, pp. 269–277, 2014.

[20] ——, "Optimization and control of one dimensional packed bed model of underground coal gasification," *Journal of Process Control*, vol. 35, pp. 11–20, 2015.

[21] A. A. Uppal, Y. M. Alsmadi, V. I. Utkin, A. I. Bhatti, and S. A. Khan, "Sliding mode control of underground coal gasification energy conversion process," *IEEE Transactions on Control Systems Technology*, 2017.

[22] A. M. Chaudhry, A. Arshad Uppal, Y. M. Alsmadi, A. I. Bhatti, and V. I. Utkin, "Robust multi-objective control design for underground coal gasification energy conversion process," *International Journal of Control*, pp. 1–8, 2018.

[23] C. B. Thorsness and J. A. Britten, "Underground coal gasification project: Final report," Lawrence Livermore National Laboratory (LLNL), California, USA, Tech. Rep. UCID- 21853, 1989.

[24] S. B. Javed, V. I. Utkin, A. A. Uppal, R. Samar, and A. I. Bhatti, "Design and implementation of multi-variable sliding mode control for

the underground coal gasification project thar," in *IEEE Control Systems Letters with Control and Decision Conference option*, vol. Under review, 2020.

[25] L. Ljung, *System Identification Theory for the User*. Switzerland: Prentice Hall PTR, 1999.

[26] H. Hjalmarsson, "System identification of complex and structured systems," *European journal of control*, vol. 15, no. 3-4, pp. 275–310, 2009.

[27] S. Gaikwad and D. Rivera, "Control-relevant input signal design for multivariable system identification: Application to high-purity distillation," in *IFAC World Congress*, vol. 349. Citeseer, 1996.

[28] M. Najafi, S. M. E. Jalali, R. KhaloKakaie, and F. Forouhandeh, "Prediction of cavity growth rate during underground coal gasification using multiple regression analysis," *International Journal of Coal Science & Technology*, vol. 2, no. 4, pp. 318–324, 2015.

[29] R. Ghosh *et al.*, "Input designs for identification of ill-conditioned multivariable systems," 2016.

[30] A. I. Bhatti, "Advanced sliding mode controllers for industrial applications," Ph.D. dissertation, Engineering, 1998.

[31] R. Pintelon and J. Schoukens, *System identification: a frequency domain approach*. John Wiley & Sons, 2012.

[32] D. Rivera, S. Gaikwad, and X. Chen, "Control-id: A demonstration prototype for control-relevant identification," in *Proceedings of 1994 American Control Conference-ACC'94*, vol. 2. IEEE, 1994, pp. 2055–2059.

[33] M. M. Rashid, P. Mhaskar, and C. L. Swartz, "Handling multi-rate and missing data in variable duration economic model predictive control of batch processes," *AIChE Journal*, vol. 63, no. 7, pp. 2705–2718, 2017.

[34] M. M. Rashid, N. Patel, P. Mhaskar, and C. L. Swartz, "Handling sensor faults in economic model predictive control of batch processes," *AIChE Journal*, vol. 65, no. 2, pp. 617–628, 2019.

[35] R. P. Pothukuchi and J. Torrellas, "A guide to design mimo controllers for architectures," 2016.

[36] S. Skogestad and I. Postlethwaite, *Multivariable feedback control: analysis and design*. Wiley New York, 2007, vol. 2.

[37] A. A. Agrachev, A. S. Morse, E. D. Sontag, H. J. Sussmann, and V. I. Utkin, *Nonlinear and optimal control theory: lectures given at the CIME Summer School held in Cetraro, Italy, June 19-29, 2004*. Springer Science & Business Media, 2008, vol. 1932.

[38] C. Thorsness and J. Britten, "Cavism user manual," Lawrence Livermore National Laboratory, CA (USA), UCID-21667, Tech. Rep., 1989.